# Wrinkle Measurement of Space Membrane Structure Under Tension Load

# Wrinkle Measurement of Space Membrane Structure Under Tension Load

By Nozomu Kogiso[1)], Aya Ito[1)] and Takashi Iwasa[2)]

[1)]*Department of Aerospace Engineering, Osaka Prefecture University, Sakai, Japan*
[2)]*Department of Mechanical Engineering, Tottori University, Tottori, Japan*

In this study, wrinkles formed in a thin membrane under tension load at corners is investigated by the wrinkle measurement experiment and the wrinkling analysis to contribute the establishment of simulation-based design methodology of a future space membrane structure. In the model experiment, a 0.4m × 0.4m square membrane model with 12.5$\mu$m thickness is set in an upright position with keeping one diagonal line horizontal to reduce the gravity effect. The bottom corner of the square membrane is fixed and the tensile forces are given at the other three corners to provide wrinkles along the diagonals. Then, wrinkle distribution is measured by a laser displacement sensor installed on the two-dimensional stage. On the wrinkling analysis, a geometrically nonlinear bifurcation analysis is adopted with a mixed interpolation of tensorial component (MITC) shell element that is known as a locking free element. Through detail investigation, the wrinkling analysis is illustrated to have sufficient accuracy. Also, the effect of large deflections around edges of membranes is discussed.

**Key Words:** Membrane, Wrinkle measurement, Geometrically Nonlinear Finite Element Analysis

## 1 Introduction

A membrane structure has great interest in the field of space structure such as a solar sail or an inflatable space antenna because of its packing efficiency and lightweight property. However, a wrinkle formed in a membrane under compressive force could cause significant deterioration in performance of the membrane structure. Therefore, it is important to design an efficient membrane shape to minimize the wrinkling.

For example, shape optimization method to minimize a wrinkle intensity in terms of the boundary edge modeled by NURBS curve was proposed [1,2)]. The wrinkle intensity is evaluated from an apparent strain energy resulting from the deformation through wrinkling based on the tension field theory[3)].

On the other hand, the wrinkling analysis based on the tension-field theory cannot evaluate the out-of-plane deformation. Though effect of the optimization using the wrinkling analysis was investigated [4)] by comparing with out-of-plane deformation obtained by a geometrically nonlinear FEM-based wrinkling analysis using a thin shell element[5,6)], the modeling accuracy is not verified sufficiently yet. In addition, establishing the simulation-based design of the space membrane structure is requited because of a large-scale space membrane structure have difficulty verifying through ground testing. Therefore, the investigation of accuracy of the wrinkling analysis is required by comparing with the experimental result.

Several methods for the out-of-plane deformation of the membrane are proposed: i.e., measurement using noncontact type sensor such as photogrammetry using CCD camera[7–9)], a capacitance proximity sensor [11)], a laser displacement sensor [6,12)] and grating projection method [10)].

In this study, accuracy of the wrinkling analysis based on thin shell theory is investigated by comparing with the wrinkle measurement experiment using a laser displacement sensor for a square membrane. Also, the effect of large deflections around edges of membranes is discussed.

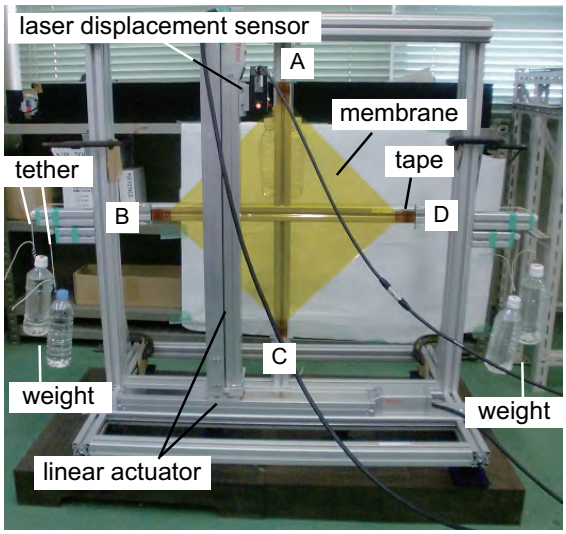


Fig. 1 Experimental equipment

Table 1 Membrane property (Du Pont-Toray Kapton 50H)

| | | |
|---|---|---|
| Young's modulus $E$ | (MPa) | 2959.6 |
| Poisson's ratio $\nu$ | | 0.34 |
| Dimension | (mm) | $400 \times 400$ |
| Thickness $t$ | ($\mu$m) | 12.5 |

## 2 Wrinkle Measurement

A 400mm-square polyimide film with thickness of 12.5$\mu$m (Du Pont-Toray Kapton 50H) is used for wrinkle measurement. Material property of the polyimide film is listed in Table 1. The square membrane is set in upright position with keeping one diagonal line horizontal on the experimental equipment to reduce the gravity effect as shown in Fig. 1. Each corner of the membrane is stiffened by polyimide tape with 30mm width and 25$\mu$m thickness and the other side of the tape is connected to a couple of tethers (Kevler supercode S-20, Hamilon) via a clasp as shown in Fig. 2. The bot-

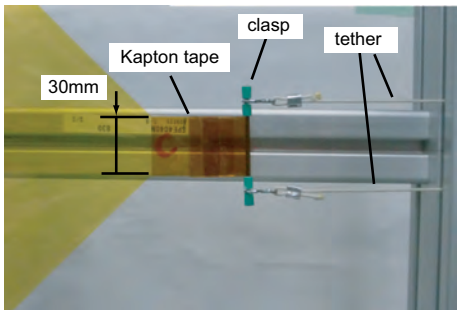


Fig. 2 Corner stiffened by polyimide tape.

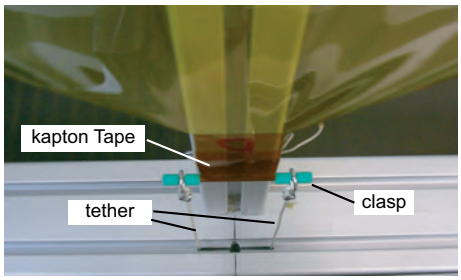


Fig. 3 Bottom corner fixed to frame.

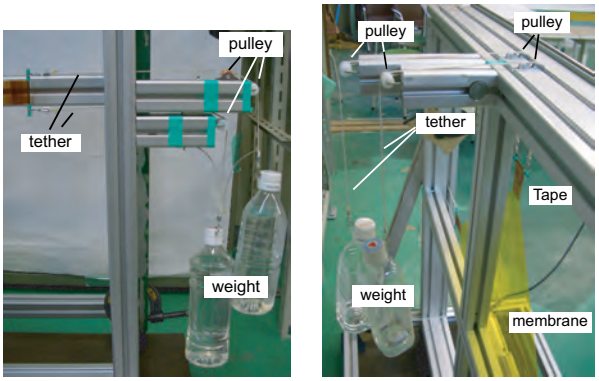


(a) Horizontal corners (b) Top corner

Fig. 4 Tension load applied at three corners.

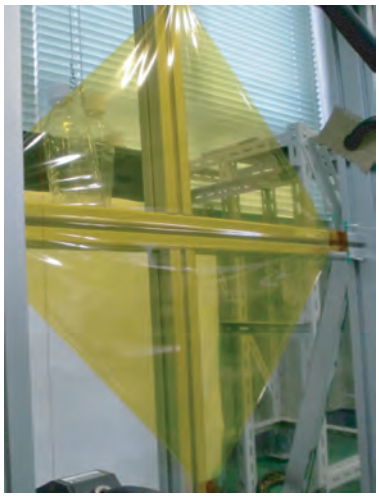

Fig. 5 Wrinkled membrane on experimental frame.

tom corner C is fixed on the frame through tethers as shown in Fig. 3 and the tension force is applied at the other three corners by weights connecting to the other side of tethers through pulleys as shown in Fig. 4. The applied weight is $T_1$ at the both horizontal

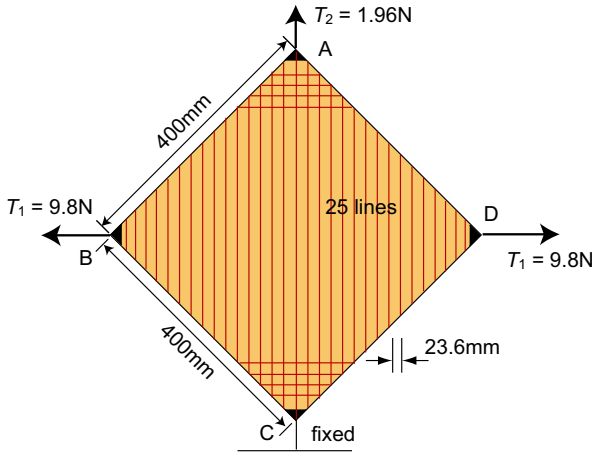


Fig. 6 Measurement positions of membrane model

corners and $T_2$ at the top corner. In this paper, the results shown is set as $T_1$ =9.8N and $T_2$ =1.96N, where the load ratio of horizontal and vertical directions is $T_1/T_2$ = 5.0. Photo of wrinkles formed in the membrane on the experimental frame is shown in Fig. 5.

The wrinkle formed in the membrane is measured by a laser displacement sensor (LK-G80, Keyence: 0.2$\mu$m of resolution limit) attached on X-Z stage system that composed of two linear actuators. Limo EZSM3E060MK, Oriental motor as vertical direction and Limo EZSM4E050MK, Oriental motor as horizontal direction. Using this stage system, the laser displacement sensor is possible to scan whole membrane area with 0.01mm of positioning accuracy, where the vertical tilt accuracy of the membrane and the X-Z stage system is adjusted to less than 0.1mm/m.

The out-of-plane deflection in the whole membrane area is measured in every 0.2mm by a laser displacement sensor along to the vertical lines. In this study, 25 measurement positions with 23.6mm distance each are selected as shown in Fig. 6. In addition, the deflection is measured along to the horizontal direction close to the top and bottom corners in order to investigate the small wrinkles formed close to the top and the bottom corners. The moving speed of the laser displacement sensor is set as slow as 10mm/sec in order to avoid the negative influence of air turbulence induced by the movement.

## 3 Wrinkling Analysis

### 3.1 Geometrically nonlinear analysis

Wrinkling phenomena are due to bifurcation and are intensely affected by small bending stiffness. Therefore, a geometrically nonlinear analysis based on the bifurcation theory is required for a detail investigation.

In this study, the wrinkling analysis is performed by using a nonlinear FEM code, FEAP (Finite Element Analysis Program) [13] with mixed interpolation of tensorial component (MITC) shell element [14]. MITC shell element is known as a locking free element and has a capability related to distortion of shell elements associated with finite deformation in nonlinear analysis. In the formulation, a finite rotation increment of directors is considered in evaluating the tangent stiffness matrices to improve the numerical stability and accuracy [6,15–17].

Introducing suitable initial imperfections in the out-of-plane direction, the post-buckling analysis is performed without any complicated perfect bifurcation analysis. For detail investigations, the

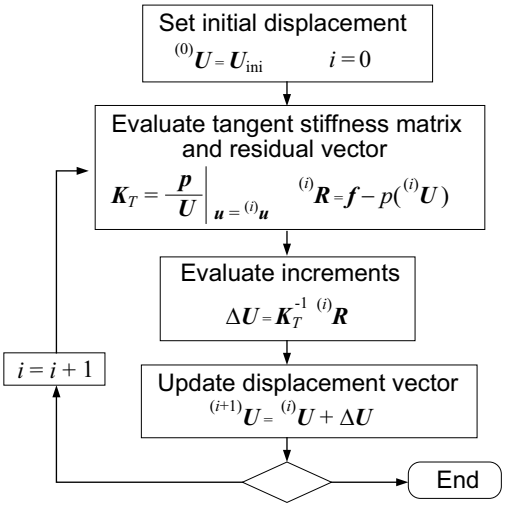


Fig. 7 Wrinkle analysis flow, $\boldsymbol{f} = \boldsymbol{p}(\boldsymbol{U})$

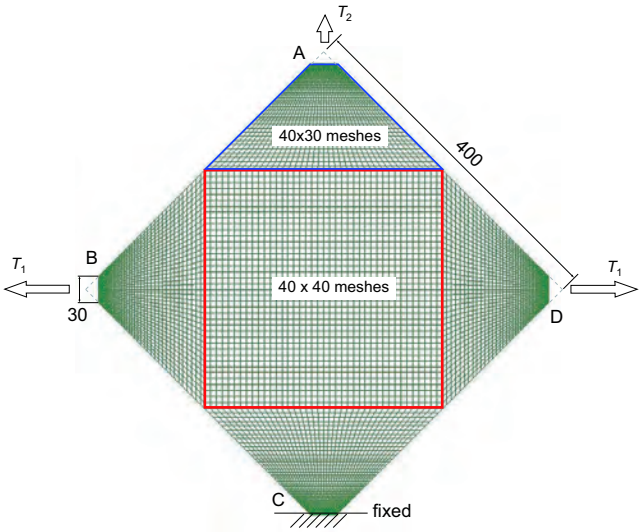


Fig. 8 FEM model of square membrane

imperfection would prefer to obtain from the experimental condition. However, it is impossible to measure the imperfection in this experimental system, because the experimental system could not keep the membrane stable without applying the tension force. Therefore, pseudo initial imperfections are introduced at all nodal points with applying normal random numbers. The magnitude of the imperfection is set to 0.1 of the membrane thickness to avoid an ill effect of the imperfection on the wrinkling analysis, that was determined from previous studies[5,6,16],

In the geometrical nonlinear analysis, Newton-Raphson method with a line-search is adopted to update the tangent stiffness matrices. Flowchart of the wrinkling analysis is illustrated in Fig. 7.

### 3.2 FEM model

In modeling the experimental condition where each corner is stiffened by polyimide tape with 30mm wide and 25$\mu$m thickness on both sides as shown in Figs. 3 and 4, the stiffened region of each corner is cut out. As shown in Fig. 8, the membrane model of an octagonal shape is discretized using four-node MITC shell elements. The number of elements is 8000 and that of nodes is 8241. A central square connecting middle-point of each edge is discretized in 40×40 square elements and the corner trapezoids are

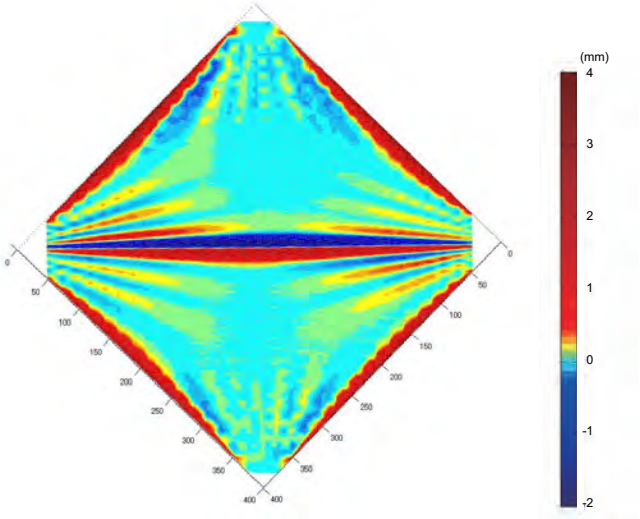


Fig. 9 Wrinkle distribution obtained by experiment

discretized in 40×30 elements where the nodal position is arranged densely to the corner to avoid the element squashed.

As boundary conditions, nodes to the bottom corner C are fixed, the tensional load $T_1$ and $T_2$ are applied at the nodes to the horizontal corners B and D, and the top corner A as distributed force, respectively.

## 4 Comparison of Experimental and Analytical Results

### 4.1 Comparison of wrinkle distributions on membrane

Wrinkle distribution result obtained by the experiment is shown in Fig. 9. Primal wrinkle with the largest amplitude is observed along the horizontal direction connecting between the left and right corners and several wrinkles with smaller amplitude are observed on both sides of the primal wrinkle around the left and the right corners. Also, smaller wrinkles appears around the top and bottom corners. This kinds of wrinkle distribution were reported in many papers [6,18,19].

In addition, along the boundary edges, larger out-of-plane deflections are observed. Such a curling of the edges is considered to naturally occur because there is no loading normal to the free edges of the membrane. Here, effect of residual deformation in preparation of the membrane specimen is considered to be negligible. When the 400mm-square specimen is cut out from the rolled product with 500mm width, the cutting force is very small such that an underlaid paper template has no scarring.

Next, the symmetric property of the experimental result is illustrated in Fig. 10. In these figures, the deflection modes of the representative symmetrical positions shown in Fig. 11 are compared, where location in horizontal axes measures in vertical direction from the top corner, A. That is, 282.8mm from the top that indicates as the thin line in each graph correspond to the horizontal diagonal, BD.

It is found that the deflections of the left and the right sides are almost identical with each other. On the other hand, the wrinkle numbers of the upper and the lower positions closed to the corners are slightly different from each other. This is considered to result from the different boundary condition that the tensional load is applied at the top corner but the bottom corner is fixed.

Then, the wrinkle distribution obtained from the analytical result is illustrated in Fig. 12. Similar to the experimental result, pri-

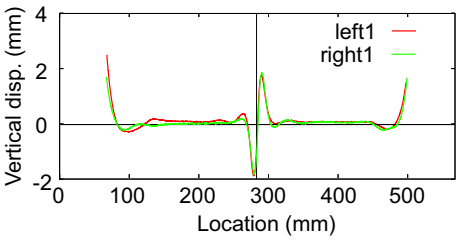


(a) left 1 and right 1

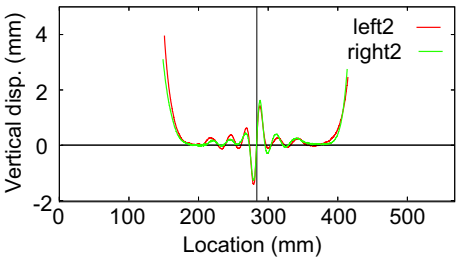


(b) left 2 and right 2

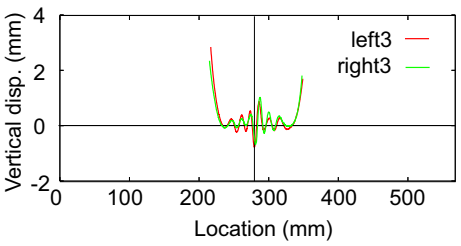


(c) left 3 and right 3

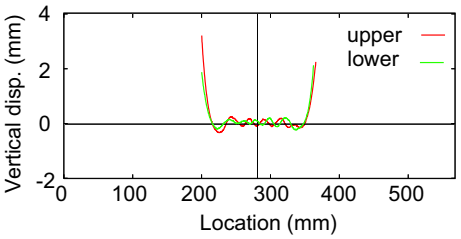


(d) lower and upper

Fig. 10 Wrinkle distribution along line segments

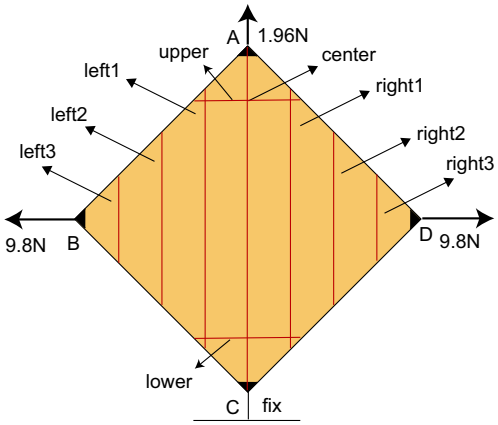


Fig. 11 Position of investigated line segments

mal wrinkle with the largest amplitude is observed along the horizontal direction connecting between the left and right corners and several wrinkles with smaller amplitude are observed on both sides of the primal wrinkle around the left and the right corners.

On the other hand, deflection mode appears on the edges is different from that of the experimental results. The deflection around edge also results from no loading normal to the free edges of the membrane. That is found from the minor stress distribution as shown in Fig. 13, where compression state ($\sigma_2 < 0$) appears along the horizontal diagonal and around both the top and the bottom corners, but along the edge, the minor principal stress is almost equal to zero.

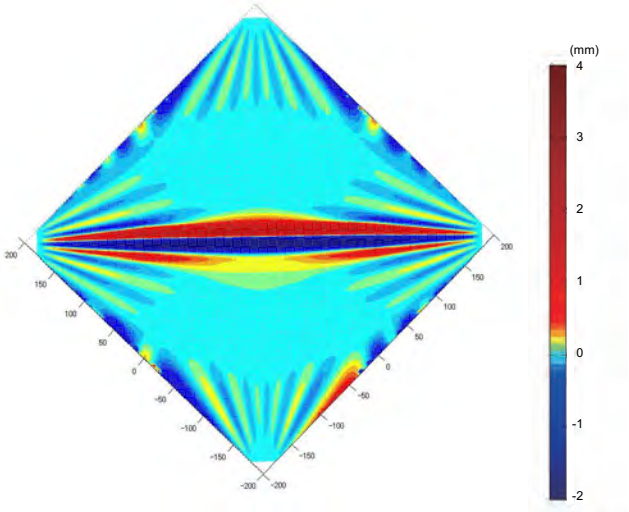


Fig. 12 Wrinkle distribution obtained by FEM analysis

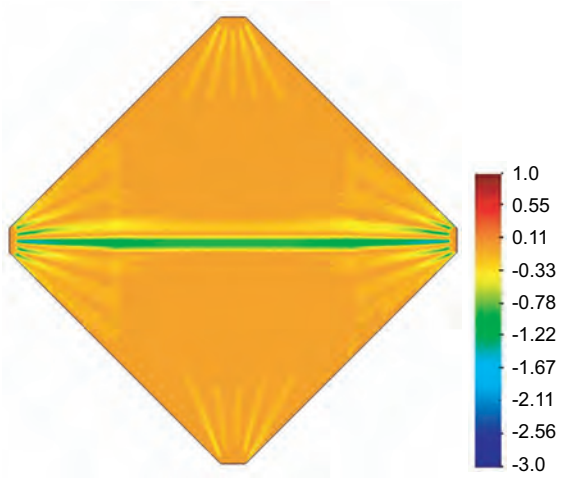


Fig. 13 Minor principal stress distribution

However, the difference of the edge deformation depends on the initial shape given randomly that might be different from the experimental condition. As discussed later, the difference has an influence on the wrinkle distribution closed to the corners, more detail modeling is required in focusing on the edge wrinkles.

Next, a detail comparison between the experiment and the analysis is described. The deflection modes along the line segments shown in Fig. 11 are compared in Fig. 14. In the figures, the experimental and the analytical results are shown in blue and red curves, respectively. A good agreement is found for the primary wrinkle shape connecting the horizontal corners B and D in each cross-section as shown in Fig. 14. However, the analytical results have slightly larger amplitude and the wavelength than the experimental results. In addition, difference of the maximum deflection around the center is larger at the negative side as compared in Table 2.

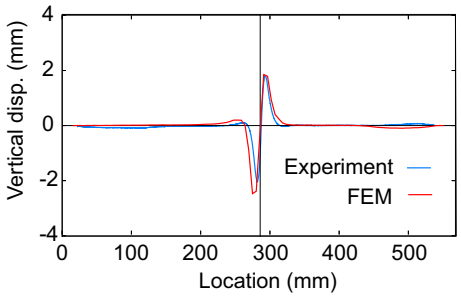


(a) center

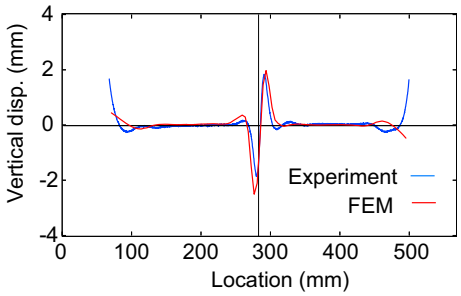


(b) right 1

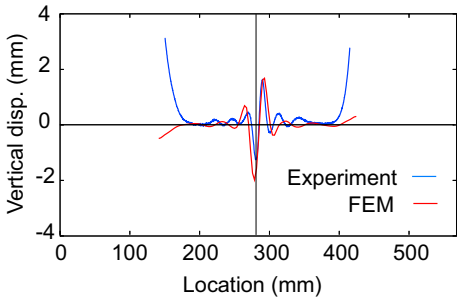


(c) right 2

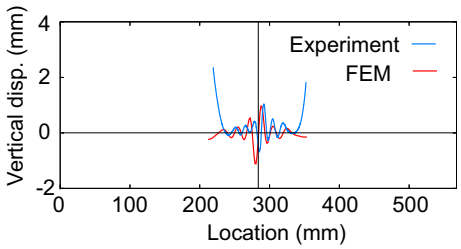


(d) right 3

Fig. 14 Comparison of wrinkle distributions along line segments

For the smaller wrinkles appears the both sides of the primary wrinkle closed to the horizontal corners, the wave number is almost identical between the experimental and analytical results as shown in Fig. 14(c), (d). However, the wrinkle mode shapes do not agree with each other. This is considered to result from difference of the large deflections around the edges. Fig. 15 compares the deflection mode between the experiment and the analysis closed to the upper and the lower corner, where the deflection curve is obtained by cutting in horizontal direction. It is found that the difference of the edge deflection causes a negative effect on the disagreement of the wrinkle distribution.

Except for the ill effect of the deflection around the edge, the analytical result is said to be a good agreement with the experimental result.

Table 2 Comparison of maximum displacement at center-line

| | Experiment | FEM analysis |
|---|---|---|
| Positive side | 1.853 | 1.706 |
| Negative side | -2.019 | -2.645 |

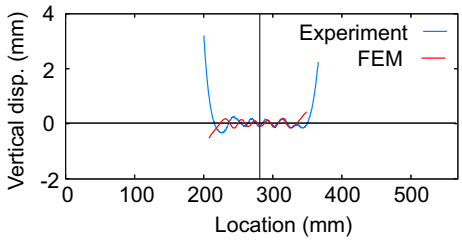


(a) upper

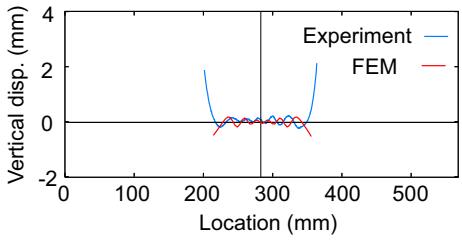


(b) lower

Fig. 15 Comparison of wrinkle distribution around top and bottom corners

### 4.2 Comparison of boundary edge deflections

Again, consider the large deflection around the edge. Effect of the deflections around the edge is negligible on the large horizontal wrinkles, but is dominant for small wrinkles around the corners as shown in Fig. 14(d).

If the deflection were mainly due to the core set, deflections around the edge would be different from adjacent edges that correspond to the rolling and the perpendicular directions, i.e., edges AB and BC . However, as shown in Fig. 10(a)~(c), deflections of the top adjacent edges, AB and AD that corresponding to the left end of the deflection curve are almost identical and deflections of the bottom adjacent edges, BC and BD that to the right end of the curve are also almost identical. That is, the large deflection around the edge is not considered to depend on core set. Rather, the deflection is considered to result from a kind of stable condition from an initial condition or gravity effect. More investigation is required for the edge deflection.

From the analytical results as Figs. 12 and 14, deflections around the edges due to slack condition is also found. However, the deflection mode is much different from the experimental result. Particularly, the singular deflection appears around the middle point of each edge as shown in Fig. 12.

It is considered that the FEM mesh has some singularity around the point. Then, wrinkling analysis using the other mesh as shown in Fig. 16, where the element discretization around the middle point is modified is performed. The obtained wrinkling distribution is illustrated in Fig. 17. The difference from the previous result is negligible. Considering the effect of the initial imperfection or more detail investigation should be required.

## 5 Concluding Remarks

This study compares the wrinkle measurement experiment and the wrinkling analysis for the square membrane under tension load

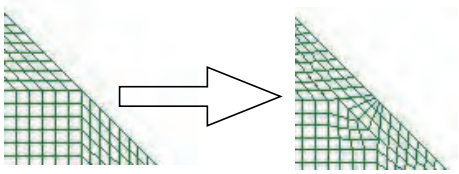

Fig. 16 Modified FEM mesh around middle point of edge

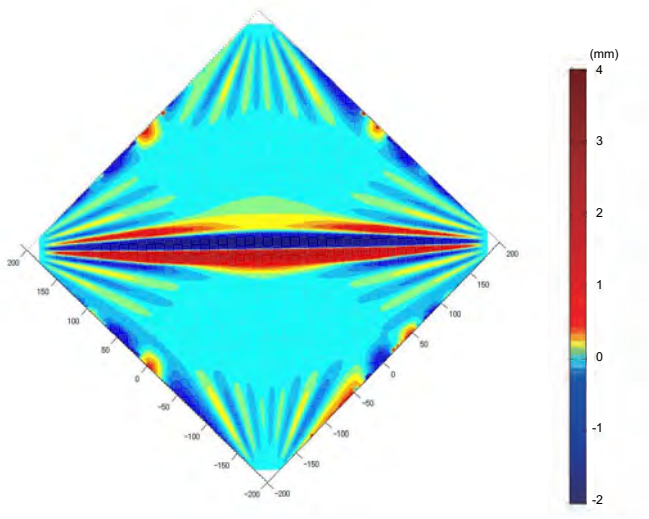


Fig. 17 Wrinkle distribution for modified mesh

in detail. On the experiment, wrinkles are measured by using the laser displacement sensor on X-Z stage, where the square membrane is set on upright position. The wrinkling analysis is performed by using a nonlinear FEM with MITC shell element.

Comparing the out-of-plane deflection distribution on the whole membrane area and the detail distribution on the specified line segments, a good agreement is obtained for the primal wrinkles between the experimental and the analytical results.

However, the accuracy is deteriorated due to deflection around the edges. Main factor of the deflection is considered as free deflection with no loadings, neither the residual deflection in unrolling or that in cutting. More detail investigations are required for the future.

**Acknowledgments**

This study was supported by "Advanced Light-weighted Structural System Research" in the "Strategic Development and Research Fund" of ISAS/JAXA. The authors also appreciate Prof. Nobuhiro Baba and Dr. Ken'ichi Kitaura from Osaka Prefecture University for their valuable advices to calibrate the experimental equipments.

**References**

1) Kogiso, N., D. Hirajo and Akita, T.: Shape Optimization of Wrinkled Region Minimization of Space Membrane, *Proc. 7th World Congress on Structural and Multidisciplinary Optimization (WCSMO-7)*, No. A0156, (2007), pp. 1-10.

2) Akita, T., and Natori, M. C.: Sensitivity Analysis Method for Membrane Wrinkling Based on the Tension-Field Theory, *AIAA J.*, **46**-6 (2008), pp. 1516-1527.

3) Akita, T., Nakashino, K., Natori, M. C., and Park, K. C.: A Simple Computer Implementation of Membrane Wrinkle Behavior via a Projection Technique, *Int. J. Number. Meth. Eng.*, **71**-10 (2007), pp. 1231-1259.

4) Akita, T., and Kogiso, N.: Boundary Shape Design of Rectangular Membrane to Reduce Wrinkling, *Research Report on Membrane Structures*, **22** (2008), pp. 15-24 (in Japanese).

5) Iwasa, T., Natori, M. C., Noguchi, H., and Higuchi, K.: Geometrically Nonlinear Analysis on Wrinkling Phenomena of a Circular Membrane, *Proc. Int. Conf. Comput. Exp. Eng. Sci. (ICCES)*, (2003)

6) Iwasa, T., Natori, M. C., and Higuchi, K.: Evaluation of Tension Field Theory for Wrinkling Analysis With Respect to the Post-Buckling Study, *T. ASME, J. Appl. Mech.*, **71**-4 (2004), pp. 532-540.

7) Blandino, J. R., Johnston, J. D., Miles, J. J., and Soplop, J. S.: Thin Film Membrane Wrinkling due to Mechanical and Thermal Loads, AIAA Paper 2001-1345 (2001).

8) Blandino, J. R., Johnston, J. D., Miles, J. J., and Dharamasi, U. K.: The Effect of Asymmetric Mechanical and Thermal Loading on Membrane Wrinkling, AIAA Paper 2002-1371 (2002).

9) Black, J. T., Leifer, J., DeMoss, J. A., and Walker, E. N.: Experimental and Numerical Correlation of Gravity Sag in Solar-Sail-Quality Membranes, *J. Spacecraft and Rockets*, **44**-3 (2007), pp. 522-527.

10) Shioji, Y., *et al.*: Shape Measurement of Metal Mesh Surface by Grating Projection Method, *Proc. 53rd Space Sciences and Technology Conference* (2009), JSASS-2009-4318 (in Japanese).

11) Jenkins, C. H., Haugen, F., and Spicher, W. H.: Experimental Measurement of Wrinkling in Membranes Undergoing Planar Deformation, *Experimental Mechanics*, **38**-2 (1998), pp. 147-152.

12) Wong, Y. W., and Pellegrino, S.: Wrinkled Membranes, Part II Analytical Models, *J. Mechanics of Materials and Structures*, **1**(1) (2006), pp. 27-61.

13) Taylor, R. L.: A Finite Element Analysis Program User Manual, ver. 8.3, http://www.ce.berkeley.edu/projects/feap/

14) Bathe, K.-J. and Dvorkin, E. N.: A Formation of General Shell Elements – The Use of Mixed Interpolation of Tensorial Components, *Int. J. Numer. Meth. Eng.*, **22** (1986), pp. 697-722

15) Jacobson, M. B., Iwasa, T. and Natori, M. C.: Quantifying Square Membrane Wrinkle Behavior Using MITC Shell Elements, AIAA 2004-174, (2004).

16) T. Iwasa, M. B. Jacobson and Natori, M. C.: Spectrum Evaluation Method for Wrinkled Membranes, *AIAA Journal*, **43**-1 (2005), pp. 194-205.

17) Noguchi, H. and Hisada, T.: An Efficient Formulation for a Shell Element Considering Finite Rotation Increments and its Assessment, *Trans. of JSME, Series A*, **58**-550 (1992), pp. 127-134. (in Japanese)

18) Wong, Y. W., and Pellegrino, S.: Wrinkled Membranes, Part I Experiments, *J. Mechanics of Materials and Structures*, **1**(1) (2006), pp. 1-25.

19) Blandino, J. R., Johnston, J. D., and Dharamsi, U. K. : Corner wrinklingof a square membrane due to symmetric mechanical loads. *J. Spacecraft Rockets*, **39**-5 (2002), pp. 717-724.

20) Wong, Y. W. and Pellegrino, S.: Wrinkled Membranes, Part III Numerical Simulations, *J. Mechanics of Materials and Structures*, **1**-1 (2006), pp. 63-95